Awake responses suggest inefficient dense coding in the mouse retina

Authors: Tom Boissonnet[1,2], Matteo Tripodi[1], Hiroki Asari*[1]

Affiliations:

1. Epigenetics and Neurobiology Unit, EMBL Rome, European Molecular Biology Laboratory, Monterotondo, 00015, Italy

2. Collaboration for joint PhD degree between EMBL and Université Grenoble Alpes, Grenoble Institut des Neurosciences, La Tronche, 38700, France

***Corresponding author:** Hiroki Asari, E-mail: asari@embl.it

Author contributions: T.B. and H.A. designed the study; T.B. and M.T. performed experiments; T.B. analyzed the results; and T.B. and H.A. wrote the manuscript.

Competing interests: The authors declare no competing financial interests.

Key words: retinal ganglion cells; in vivo recordings; awake; anesthesia; efficient coding.

Acronyms: CMOS, complementary metal-oxide semiconductor; DS, direction-selectivity; dLGN, dorsal lateral geniculate nucleus; DLP, digital light processing; FMM, fentanyl, medetomidine and midazolam; GABA, gamma-aminobutyric acid; LED, light emitting diode; OS, orientation-selectivity; OT, optic tract; PCA, principal component analysis; PFA, paraformaldehyde; RGC, retinal ganglion cells; SC, superior colliculus; STA, spike-triggered average; UV, ultraviolet.

Abstract

The structure and function of the vertebrate retina have been extensively studied across species with an isolated, *ex vivo* preparation. Retinal function *in vivo*, however, remains elusive, especially in awake animals. Here we performed single-unit extracellular recordings in the optic tract of head-fixed mice to compare the output of awake, anesthetized, and *ex vivo* retinas. While the visual response properties were overall similar, we found that awake retinal output had 1) faster kinetics with less variability in the response latencies across different cell types; and 2) higher firing activity, by ~20 Hz on average, for both baseline and visually evoked responses. Notably, unlike the other conditions, many awake ON cells did not increase firing in response to light increments due to high baseline activity near saturation. Instead, they encoded light intensity fluctuations primarily by decreasing firing upon light decrements. In either condition, the visual message remains the same: the more spikes, the higher light intensity. The awake response patterns, however, violate efficient coding principles, predicting that sensory systems should favor firing patterns minimizing energy consumption. Our findings suggest that the retina employs dense coding *in vivo*, rather than sparse efficient coding as suggested from previous *ex vivo* studies.

Introduction

The vertebrate retina is one of the best characterized parts of the central nervous system (Gollisch and Meister, 2010; Masland, 2012). It consists of ~100 cell types in total (Shekhar et al., 2016; Yan et al., 2020), including ~30 types of retinal ganglion cells (RGCs) that send the retinal output signals to the brain via the optic nerve (Sanes and Masland, 2015; Baden et al., 2016). Each of these RGC types forms distinct neural circuits within the retina to extract specific features of the visual image coming into the eye, such as color, contrast, and motion. The retina thus performs parallel and dynamic processing as the first stage of the visual pathway.

Most of our knowledge on retinal function has been obtained from *ex vivo* studies because isolated retinal tissues are nevertheless functional, i.e., responsive to light (Barlow et al., 1964). While powerful, however, *ex vivo* physiological approaches have certain limitations. First, one cannot perform long-term recordings (Meister et al., 1994). Second, one cannot avoid artifacts due to retinal dissection, such as the effect of cutting RGC axons (Vidal-Sanz et al., 2017) or retinal epithelial detachment (Strauss, 2005). Neuromodulatory effects of retinopetal pathways are also difficult to study in an isolated retinal preparation (Repérant et al., 2006; Esposti et al., 2013). *In vivo* studies are thus indispensable for clarifying retinal function thoroughly.

Previous physiological studies on the retina *in vivo* were conducted mostly under anesthetized—and often paralyzed—conditions. To monitor RGC activity *in vivo*, for example, single-unit recordings were made directly from the retina (Kuffler, 1953), at the optic nerve or tract fibers (Hartline, 1938; Lettvin et al., 1959; Enroth-Cugell and Robson, 1966; Mastronarde, 1983, 1985; Sagdullaev and McCall, 2005), or in the form of “slow-potential” in the dorsal lateral geniculate nucleus (dLGN; Bishop et al., 1962; Kaplan and Shapley, 1984). Optical methods were also developed to image the activity of retinal neurons directly through the pupil of a live animal (Geng et al., 2012; Yin et al., 2013, 2014). In contrast, thus far only a handful of studies have reported awake recordings from the retina (Esposti et al., 2013; Hong et al., 2018) or its outputs (Weyand, 2007; Liang et al., 2018, 2020; Schröder et al., 2020; Sibille et al., 2021). Thus, despite a long history of research on the retina, it still remains unclear what exactly the eye tells the brain in awake animals.

As recordings from awake behaving animals became routine for many brain areas (Dombeck et al., 2007; Jun et al., 2017), growing attention has been paid to the roles of an animal’s behavior and internal brain states in the function of the sensory systems (Niell and Stryker, 2010; Lee and Dan, 2012). For example, systematic studies on the early visual pathway showed higher firing activity and faster response dynamics in both dLGN (Durand et al., 2016) and the superior colliculus (SC; De Franceschi and Solomon, 2018) of awake

53 animals than those under anesthesia. A critical question that was left unanswered is to what
54 extent such differences originate in the retina.

55 To clarify differences in the retinal visual response properties between awake and
56 anesthetized conditions, here we employed single-unit extracellular recording techniques from
57 head-fixed mice. Specifically, the electrodes were placed in the optic tract (OT), a bundle of
58 nerve fibers composed of RGC axons as they project from the eye to their main targets: dLGN
59 and SC. These recordings are superior to direct *in vivo* retinal recordings (e.g., with epiretinally
60 implanted mesh electrodes; Hong et al., 2018) because the retinal circuits and the eye optics
61 remain intact, and also to those extracellular recordings in SC (Sibille et al., 2021) or dLGN
62 (Weyand, 2007) because RGC axonal signals do not need to be disambiguated from those of
63 local axons or somata. This advantage also exists for calcium imaging recordings of the retina
64 directly in the eye of immobilized zebrafish larvae (Esposti et al., 2013) or those of RGC axon
65 terminals in dLGN (Liang et al., 2018, 2020) or SC (Schröder et al., 2020). These imaging
66 approaches, however, lack the temporal precision as in the electrophysiology, which is an
67 important aspect of the information processing in the retina (Gollisch and Meister, 2008).

68 From our OT recordings, we examined the visual responses to a set of visual stimuli
69 widely used for probing retinal function *ex vivo* (Baden et al., 2016; Jouty et al., 2018),
70 including moving gratings, white-noise stimuli, and full-field flickering stimuli at different
71 temporal frequencies. We used two different anesthetics that are commonly used in
72 neuroscience research: isoflurane gas and an intraperitoneal combination of fentanyl,
73 medetomidine and midazolam (FMM). In both cases, we found that the temporal dynamics of
74 the retinal outputs were slower than in awake recordings, consistent with the previous studies
75 on the effects of anesthesia in retinorecipient areas (dLGN, Durand et al., 2016; SC, De
76 Franceschi and Solomon, 2018). We also found that the retinal outputs in an awake condition
77 had higher baseline firing rates than in anesthetized or *ex vivo* conditions. As expected from
78 previous *ex vivo* studies (Masland, 2012; Sanes and Masland, 2015; Baden et al., 2016; Jouty
79 et al., 2018), anesthetized ON cells encoded light increments by increasing firing from their

low baseline firing rates. In contrast, many awake ON cells encoded light decrements by decreasing firing from their high baseline firing rates, but not light increments due to saturation. They convey the same information in either condition: the more spikes, the higher light intensity. However, the amount of information transmitted per spike is lower in the awake responses. This disagrees with sparse efficient coding (Attneave, 1954; Barlow and Rosenblith, 1961) or minimum energy principles (Laughlin, 2001) that are widely used as a model of the early visual processing (Atick and Redlich, 1990; Gjorgjieva et al., 2019). A new theoretical framework based on dense coding principles will thus be needed to explain retinal function *in vivo*.

Results

Characterization of retinal output responses *in vivo*

To monitor retinal output *in vivo*, we established extracellular single-unit recording methods from axons of retinal ganglion cells (RGCs) in the optic tract (OT) of head-fixed mice (Figure 1). In total, we made 17 chronic (75 cells) and 52 acute recordings (298 cells with isoflurane; 103 cells with FMM), where a standardized set of visual stimuli were presented to the subject animal to characterize the visual response properties of the recorded cells (for ~1 hour; Figure 1A,B; see Methods for details).

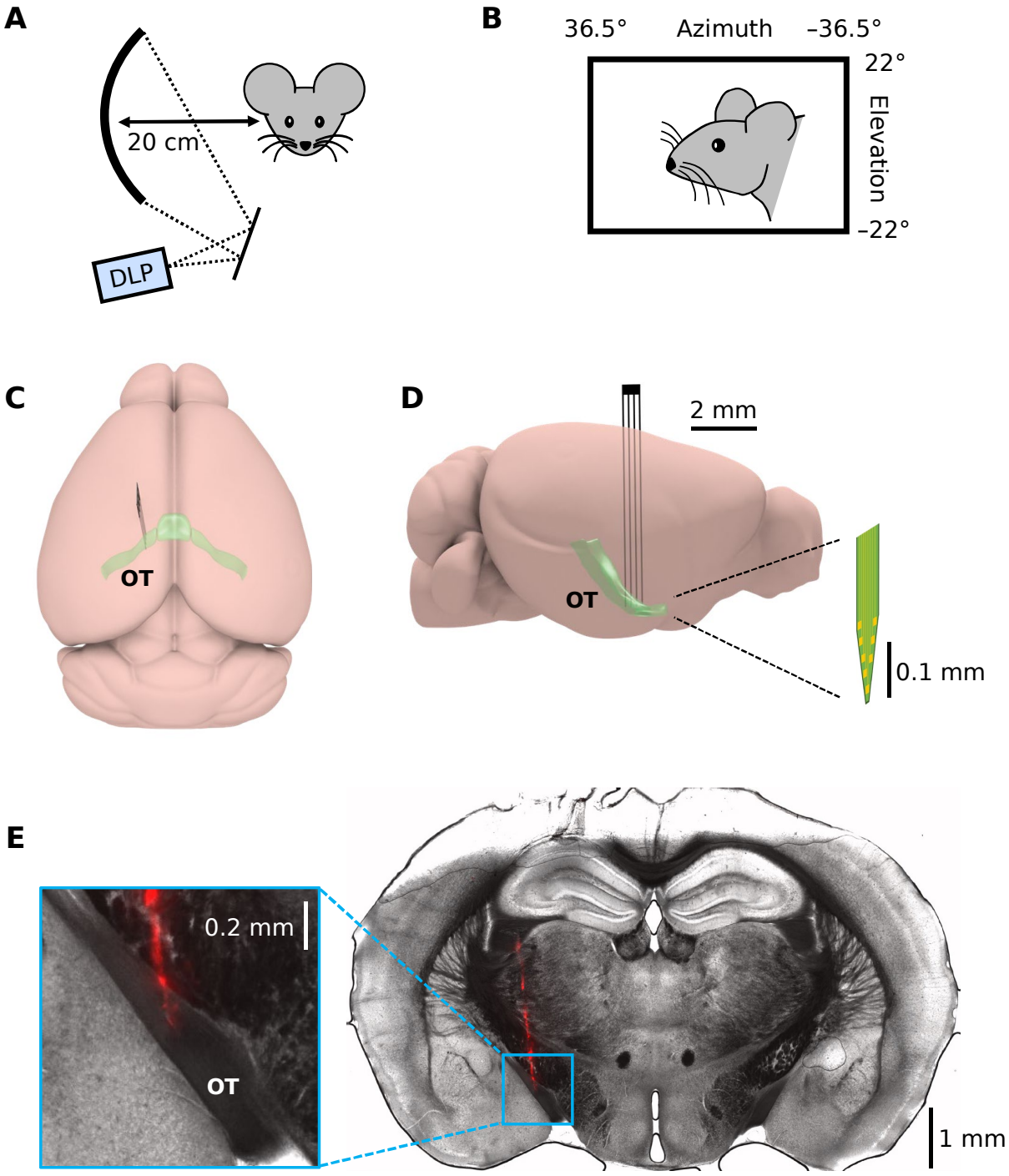

Figure 1: *in vivo* extracellular recordings from the mouse optic tract. *A,B*: Schematic diagram of the experimental set-up. We presented visual stimuli to a head-fixed mouse using a digital light processing (DLP) device projecting images onto a spherical screen placed laterally to the subject animal (A, front-view; B, side-view). See Methods for details and specifications. *C,D*: Schematic diagram (C, top-view; D, side-view) of the brain and electrode location to target the optic tract (OT). *E*: Histological image of a representative brain sample (coronal section, 150 µm thick) showing the electrode trace (red, DiI stain deposited on the electrode).

We performed physiological cell-type classification of the recorded cells (see Methods for details) and identified most major RGC types in our data sets (Figure 2; Sanes and Masland, 2015; Baden et al., 2016; Jouty et al., 2018). Specifically, we first identified reliably responsive cells based on the visual responses to full-field contrast-inverting stimuli (Figure 2A,B), and categorized their response polarity into ON, ON/OFF, OFF types (Figure 2C). In both anesthetized and awake conditions, we found around 30-50% of ON cells, 10-30% of ON/OFF cells, and around 20% of OFF cells in our data sets. We then further classified the cells from the viewpoint of motion sensitivity, based on the responses to moving gratings in eight different directions (Figure 2D-F). In the anesthetized conditions, about a half of the cells (42-56%) were motion sensitive regardless of their response polarities or anesthetics. In contrast, we found much less motion sensitive cells (15%) in the awake condition. This is consistent with the previous results in the superior colliculus (SC; Kasai and Isa, 2021), and presumably due to the consequence of optokinetic nystagmus (Kretschmer et al., 2017). When a motion in a wide visual field is presented, such as moving gratings, mice show compensatory eye movements to stabilize the image on the retina (Tabata et al., 2010). As a result, motion sensitive RGCs might have been driven less in the awake condition.

Our approach cannot obtain some RGC types that do not send their axons to OT, such as the one projecting to the suprachiasmatic nucleus via the retinohypothalamic tract (Li and Schmidt, 2018). Nevertheless, the fact that we obtained diverse types of visual responses, better than previous *in vivo* studies (Hong et al., 2018; Liang et al., 2018; Schröder et al., 2020; Sibille et al., 2021) if not all the ~30 RGC types observed *ex vivo* (Baden et al., 2016; Jouty et al., 2018), validates our recording methods to monitor retinal outputs *in vivo*.

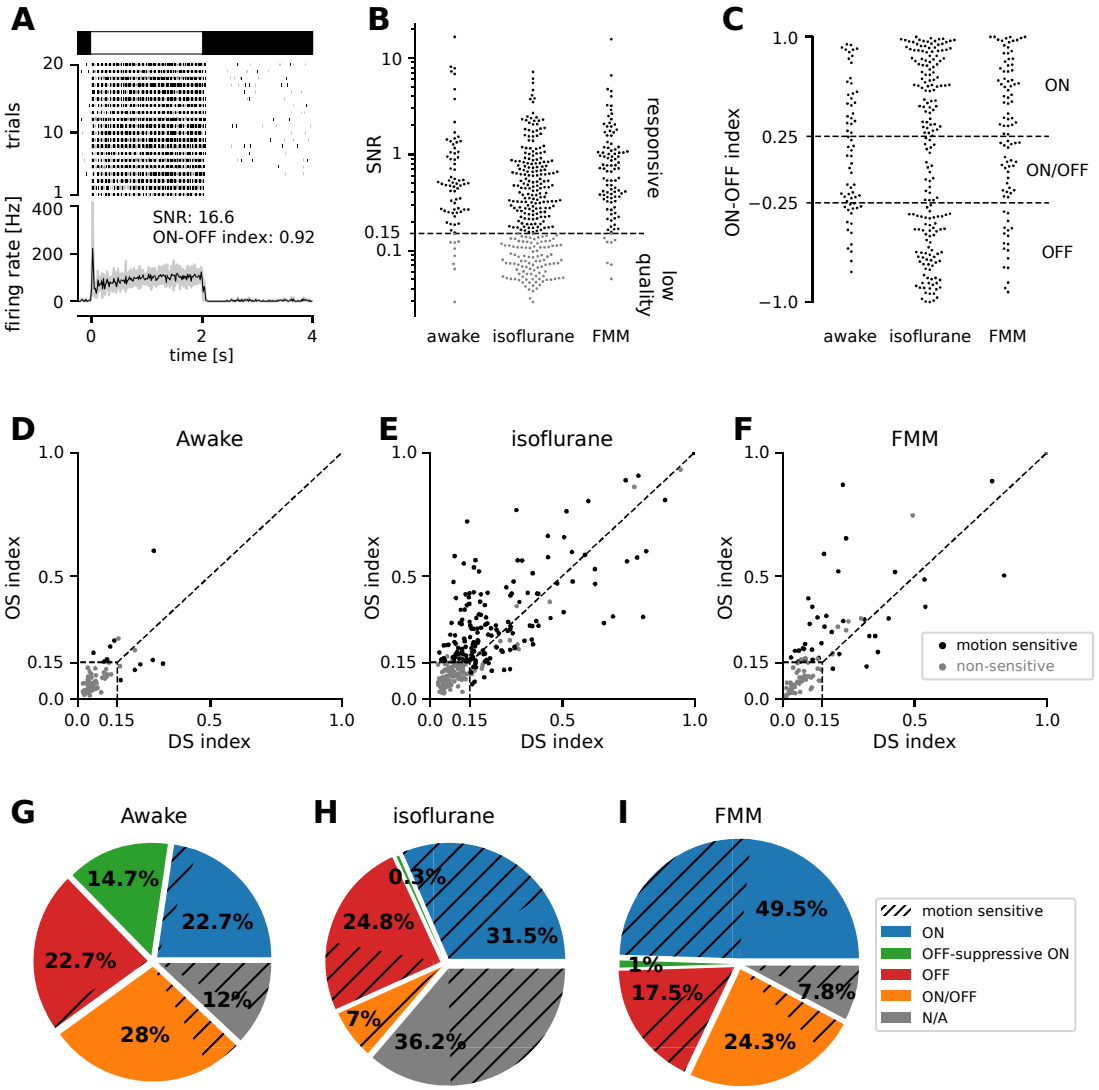

Figure 2: Physiological classification of retinal output responses *in vivo*. *A*: Representative retinal output responses to full-field contrast inverting stimuli: top, stimulus; middle, raster graph over trials; bottom, peri-stimulus time histogram (black, mean; gray, variance; signal-to-noise ratio (SNR), Eq.(1) in Methods; ON-OFF index, Eq.(2)). *B*: SNR of the retinal output responses in different recording conditions. We set a threshold at 0.15 to identify reliably responsive cells (black) and low-quality unclassifiable cells (gray). *C*: ON-OFF index distributions from the reliably responsive cells. While no apparent clusters were identified, we set a threshold at ±0.25 to categorize the response polarity into ON, ON/OFF, and OFF types. Within the ON cell type, we further identified an OFF-suppressive type based on the full-field flickering stimulus responses (Figure 3). *D-F*: Distribution of DS/OS indices (Eq.(3)) in each recording condition (D, awake; E, isoflurane; F, FMM). We set a threshold at 0.15 (with p<0.2) to identify motion sensitive (black) and non-sensitive (gray) cells. *G-I*: Fraction of identified cell types *in vivo*: ON (blue; OFF-suppressive type in green), OFF (red), ON/OFF (orange), and the rest unclassifiable cells ("N/A", gray). Cells in each category were further divided based on the motion selectivity (hatched). The OFF-suppressive ON cells were prominent in the awake condition (G, 11/75 cells), but rarely observed under anesthesia (H, isoflurane, 1/298 cells; I, FMM, 1/103 cells).

Higher firing in awake than in anesthetized mice

For characterizing the retinal output properties *in vivo*, we first analyzed the responses to full-field sinusoidally flickering stimuli that linearly changed the amplitude over time (from 0 to 100% contrast for 10 s; see Figure 3A-C for representative responses). An even power of sine function with a sigmoid envelope generally fitted well to the responses (Eq. (6) in Methods). We then focused on the parameter values to analyze the response properties in different recording conditions.

First, we found significantly higher baseline firing rates in awake mice (18 ± 26 Hz; median ± interquartile range) than in those under anesthesia (isoflurane, 2 ± 6 Hz, $p < 0.001$, *U*-test; FMM, 2 ± 4 Hz, $p < 0.001$; Figure 3D). Awake ON cells had particularly high baseline activity (up to ~100 Hz) and showed a prominent reduction in firing rates in response to light decrements (see Figure 3B for example). In contrast, due to this high baseline activity near saturation, many of them showed virtually no responses to light increments ($N = 11/28$), except for a sharp rebound response to a full-contrast inversion ($N = 8/11$; see Figures 2A and 3B for example). These ON cells had negative amplitudes in the curve fit (Figure 3E, green) with the same response phase as OFF cells (Figure 3F; see Figure 3A for a representative OFF cell's responses). This indicates that they primarily encode light decrements by decreasing firing from their high baseline firing rates (61 ± 27 Hz, mean ± standard deviation), rather than light increments by increasing firing as conventional ON cells do (Masland, 2012; Sanes and Masland, 2015; Baden et al., 2016; Jouty et al., 2018). We thus categorized these cells independently as an "OFF-suppressive" ON type (Figure 2G). This is a new response type likely emerged due to high baseline firing in awake mice. Indeed, such responses were barely observed in anesthetized animals (isoflurane, 1/298 cells; FMM, 1/103 cells; Figure 2H,I) where the baseline firing rate was generally low (Figure 3D). As expected from previous *ex vivo* studies (Masland, 2012; Sanes and Masland, 2015; Baden et al., 2016; Jouty et al., 2018), anesthetized ON cells increased firing upon light increments (see Figure 3C for a representative response). Positive amplitudes in the curve fit (Figure 3E) with

an opposite response phase from OFF cells (Figure 3F) further support that these ON cells encode light increments. Taken together, these data suggest that the retinal coding depends on the baseline firing level of RGCs.

To characterize contrast sensitivity, we next examined the estimated response magnitude at 10% contrast from the sigmoid function used in the curve fit (Eq.(6)), and found no significant differences across the recording conditions (awake, 4 ± 10 Hz, median ± interquartile range; isoflurane, 6 ± 13 Hz; FMM, 3 ± 10 Hz; $p = 0.13$, Kruskal-Wallis test). Nevertheless, the midpoint of the sigmoid was larger in awake cells ($67 \pm 43\%$ contrast, median ± interquartile range) than in anesthetized ones (isoflurane, $45 \pm 44\%$, $p < 0.001$, Mann-Whitney *U*-test; FMM, $43 \pm 38\%$, $p = 0.002$) so was the plateau (absolute value of peak evoked firing rate, Figure 3E; awake, 52 ± 68 Hz, median ± interquartile range; isoflurane, 37 ± 33 Hz, $p = 0.03$, Mann-Whitney *U*-test against awake data; FMM, 35 ± 34 Hz; $p = 0.007$). This indicates a larger dynamic range in the awake condition, while contrast sensitivity itself remains largely unchanged.

Finally, we found a significant phase shift in the responses between the recording conditions (Figure 3F). This phase parameter in the curve fit represents the position of the response peak relative to the sinusoidal stimulus intensity patterns (see Methods for details), and we identified two clusters in each data set: the one with negative phase for ON cells (Figure 3F, blue) and the other with positive phase for OFF and OFF-suppressive ON cells (Figure 3F, red and green, respectively). ON/OFF cells were found in either cluster, depending on the relative strength of their responses to light increments versus light decrements (Figure 3F, orange). In both clusters, we found that the phase was on average smallest for the awake condition (-2.4 ± 0.3 and 1.5 ± 0.3 radian, respectively; mean ± standard deviation; isoflurane, -0.8 ± 0.5 and 2.0 ± 0.5 radian; $p < 0.001$ for both cases, *t*-test), while largest for the FMM anesthesia (-0.2 ± 0.8 and 2.6 ± 0.6 radian; $p < 0.001$ for both cases against corresponding isoflurane data). This implies that the response dynamics are faster in awake mice than those under anesthesia, especially with FMM.

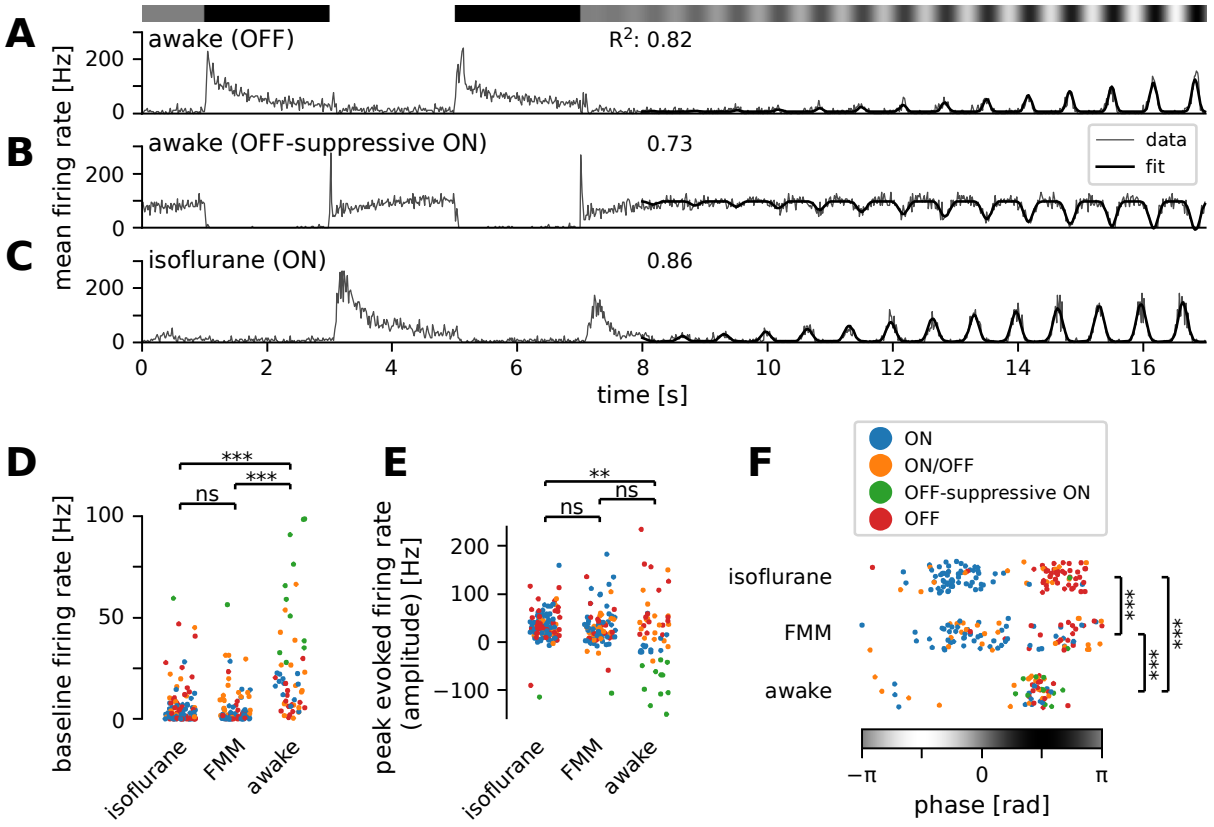

Figure 3: Many ON retinal ganglion cells showed suppressive OFF responses in awake condition. *A-C*: Mean firing rate of representative cells in response to a sinusoidally-flickering stimulus with increasing contrast in the awake (A, OFF; B, OFF-suppressive ON, the same cell as in Figure 2A) or anesthetized conditions (C, ON). Overlaid with the peri-stimulus time histogram (gray) is the model fit (black, Eq.(6) in Methods). The number on top indicates the fit quality (explained variance R^2 in Eq.(5)). *D-F*: population data of the model parameters (D, baseline B; E, amplitude A; F, phase ϕ) across different conditions: isoflurane anesthesia ($N = 103$), FMM anesthesia ($N = 92$) and awake ($N = 51$). The sinusoidal stimulus pattern relative to the response peak is also indicated at the bottom of F. Cell types are color-coded as in Figure 2 (blue, ON; green, OFF-suppressive ON; red, OFF; orange, ON/OFF). Note high baseline with negative amplitude and positive phase for the OFF-suppressive ON cells, which were predominantly found in the awake condition: ***, $p < 0.001$; **, $p < 0.01$; ns, non-significant (D, *U*-test; E, *F*-test; F, *t*-test).

Faster response kinetics in awake than in anesthetized mice

To better characterize the kinetics of retinal output *in vivo*, we next analyzed the responses to full-field sinusoidal flickers at different temporal frequencies (Figure 4). In awake mice, most cells responded faithfully to all the stimulation frequencies we tested from 1.875 to 15 Hz (see Figure 4A for example). Some awake cells showed the largest responses to the 15 Hz stimulation (Figure 4A; curve fit in violet, Eq. (4)), suggesting that they were possibly tuned to even higher frequencies. In the anesthetized conditions, in contrast, retinal output responses typically followed the stimulation frequencies up to 7.5 Hz, but failed to do so at 15 Hz (see Figure 4B for example). For quantification, we fitted an even power of sine function to the responses (Eq.(4) in Methods) and set a threshold of the curve fit quality (defined as the explained variance; Eq.(5)) at 0.2 to select cells with robust responses (Figure 4C,D). In the awake condition, a larger number of cells responded well at medium frequencies (3.75 Hz, 75%; 7.5Hz, 82%) than at a low frequency (1.875 Hz, 60%); and the majority of the awake cells remained responsive to a high frequency stimulus (15 Hz, 58%). Under anesthesia, in contrast, the fraction of responsive cells was the largest at a low frequency (1.875 Hz; isoflurane, 85%; FMM, 67%). Fewer cells responded robustly at faster flicker rates (3.75 Hz and 7.5 Hz; isoflurane, 73% and 65%, respectively; FMM, 63% and 59%), and only a small fraction of the anesthetized cells were able to follow the stimulation frequency at 15 Hz (isoflurane, 9%; FMM, 3%). Consistent with the phase analysis results described above (Figure 3F), these outcomes indicate that the retinal output dynamics are faster in awake animals than those under anesthesia, especially for FMM.

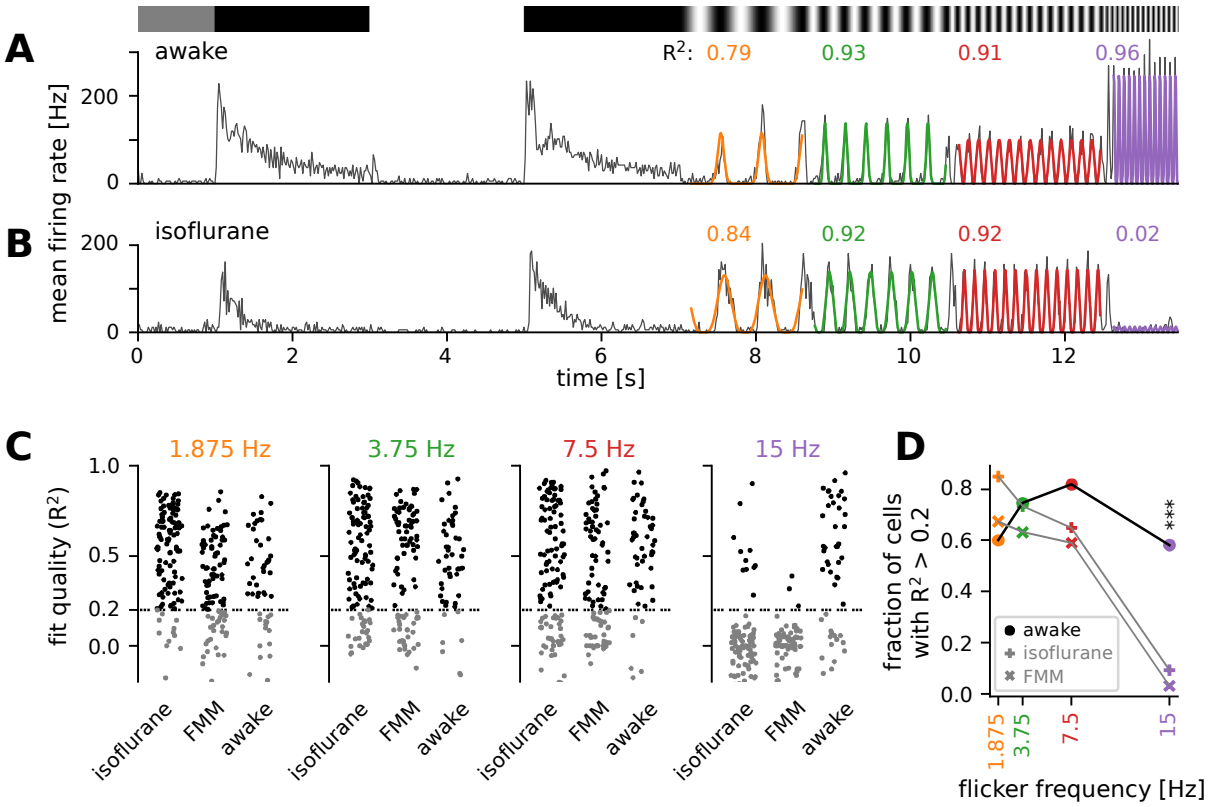

Figure 4: Retinal output showed higher temporal frequency sensitivity in awake than in anesthetized mice. *A*: Representative retinal output (black, mean firing rate over 10 trials) in an awake condition in response to full-field sinusoidally flickering stimuli at different temporal frequencies (1.875, 3.75, 7.5 and 15 Hz), following full-field contrast inversions. Overlaid is the curve fit (Eq.(4) in Methods) in different colors. The number on top is the explained variance of the curve fit (R^2, Eq. (5) in Methods) in corresponding colors, representing the fit quality. *B*: Representative retinal output responses under isoflurane anesthesia (shown in the same format as in A). *C*: Population data of the fit quality at four different stimulus frequencies in the awake ($N = 51$) or anesthetized conditions (isoflurane, $N = 103$; FMM, $N = 92$). The fit quality threshold was set to be 0.2 (black, $R^2 \geq 0.2$; gray, $R^2 < 0.2$). *D*: Fraction of the cells with the fit quality above the threshold across different conditions (awake, black line with circles; isoflurane, gray line with vertical crosses; FMM, gray line with diagonal crosses), representing the frequency tuning of the retinal output at the population level. A significantly larger fraction of cells was responsive at 15 Hz in the awake condition than in the anesthetized conditions (***, $p < 0.001$ for both isoflurane and FMM; two-proportion *z*-test).

Comparison of retinal output properties between *in vivo* and *ex vivo*

We have thus far focused on the retinal output properties *in vivo*, and showed higher baseline firing rates (Figure 3) and faster response kinetics (Figure 4) in awake mice than in those under anesthesia. We next asked if RGC responses differ between *in vivo* and *ex vivo* conditions. This is a critical comparison because retinal physiology has been mostly studied and best characterized in an isolated preparation (Gollisch and Meister, 2010; Sanes and Masland, 2015), but little is known about it in awake animals (Weyand, 2007; Liang et al., 2018, 2020; Schröder et al., 2020; Sibille et al., 2021). Here we exploited stimulus ensemble statistical techniques ("reverse correlation"; Meister et al., 1994; Chichilnisky, 2001) to systematically characterize the visual response properties and make a direct comparison across different recording conditions in the linear-nonlinear cascade model framework (see Methods for details). Specifically, using full-field white-noise stimuli, we analyzed 1) the linear temporal filter (Figure 5), estimated by the spike-triggered average (STA) stimulus, i.e., the mean stimulus that triggered spiking responses; and 2) the static nonlinear gain function (Figure 6), i.e., an instantaneous mapping of the STA output to the neural responses (Eq. (7) in Methods). Here we reanalyzed the existing data sets for *ex vivo* recordings (696 cells from 18 isolated mouse retinas; Vlasiuk and Asari, 2021).

Faster response kinetics in awake condition than *ex vivo*

We identified a good quality STA in more than two-thirds of the cells recorded *in vivo* (e.g., Figure 5A). To compare the temporal dynamics of the STAs across different recording conditions, we used the following two measures: 1) the first peak latency of the STA estimated from a difference-of-Gaussian curve fit (Figure 5A); and 2) spectral peak frequency calculated by the Fourier transform of the fitted curve (Figure 5B). Consistent with the results measured by the flickering stimuli at different frequencies (Figure 4), we found faster kinetics in awake animals than in anesthetized ones (Figure 5C,D): i.e., significantly shorter peak latencies

(awake, 35 ± 12 ms, mean ± standard deviation; isoflurane, 79 ± 18 ms, $p < 0.001$, *t*-test; FMM, 87 ± 24 ms, $p < 0.001$; Figure 5C) and higher peak frequencies (awake, 9.6 ± 3.0 Hz; isoflurane, 4.6 ± 1.6 Hz, $p < 0.001$; FMM, 3.7 ± 1.2 Hz, $p < 0.001$; Figure 5D). Interestingly, we identified that the *ex vivo* data lied in-between. The *ex vivo* STAs had significantly longer peak latencies (64 ± 28 ms, $p < 0.001$) and lower peak frequencies (4.3 ± 1.8 Hz, $p < 0.001$) than the awake ones. In contrast, the peak latencies were significantly shorter in an isolated retinal preparation than in the anesthetized conditions (isoflurane, $p < 0.001$; FMM, $p < 0.001$), while the peak frequencies were comparable between these conditions (isoflurane, $p = 0.7$; FMM, $p = 0.052$).

We further analyzed the STA dynamics across different cell types. For clustering the STAs obtained in each recording condition, we used the principal component analysis (PCA; see Methods for details). As in previous *ex vivo* studies (Gollisch and Meister, 2008; Asari and Meister, 2014), the first two principal components accounted for most of the variance (78-86%, collectively), and the four quadrants of the PCA biplot generally represented distinct filter shapes, corresponding to monophasic OFF (mono-OFF), biphasic OFF (bi-OFF), monophasic ON (mono-ON), and biphasic ON (bi-ON) response types, respectively. In all recording conditions, no apparent cluster was found in this feature space, leading to a continuum of the STA shape patterns across populations (Figure 5E-H). Nevertheless, we identified two features that were different between *ex vivo* and *in vivo*, especially distinct in the awake condition. First, while the monophasic types were generally slower than the biphasic types, differences in the peak latencies were much larger in the *ex vivo* (Figure 5G; mono-ON 83 ± 24 ms versus bi-ON 58 ± 31 ms, $p < 0.001$, *t*-test; mono-OFF 67 ± 29 ms versus bi-OFF 48 ± 8 ms, $p < 0.001$) or anesthetized conditions (Figure 5E, isoflurane: mono-ON 91 ± 22 ms, bi-ON 67 ± 6 ms, $p < 0.001$; mono-OFF 89 ± 14 ms, bi-OFF 68 ± 8 ms, $p < 0.001$; Figure 5F, FMM: mono-ON 97 ± 30 ms, bi-ON 78 ± 11 ms, $p = 0.051$; mono-OFF 103 ± 13 ms, bi-OFF 70 ± 11 ms, $p < 0.001$) than in the awake condition (Figure 5H; mono-ON 40 ± 7 ms, bi-ON 30 ± 13 ms, $p = 0.03$; mon-OFF 39 ± 7 ms, bi-OFF 34 ± 14 ms, $p = 0.2$). Second, we found

that ON cells were significantly slower than OFF cells *ex vivo* (mono-ON versus mono-OFF, $p = 0.002$; bi-ON versus bi-OFF, $p = 0.03$), but not *in vivo* ($p > 0.2$ in all the conditions examined). Taken together, our results suggest that awake responses are faster and their kinetics are more similar across different cell types than *ex vivo* or anesthetized responses.

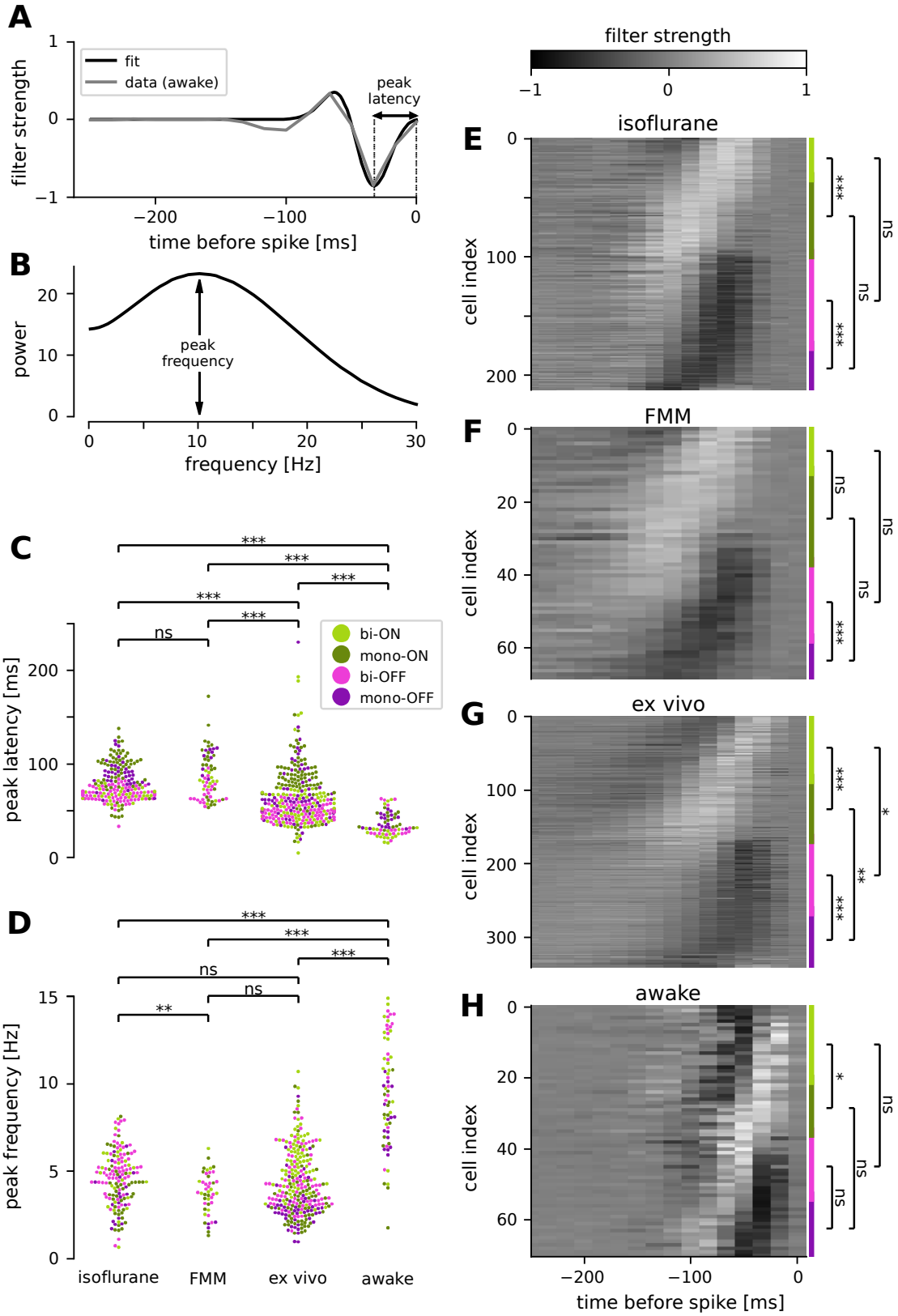

Figure 5: Retinal ganglion cells showed faster response dynamics in awake condition than in anesthetized or *ex vivo* conditions. *A*: Temporal filter of a representative awake cell (gray, spike-triggered average (STA) of the full-field randomly flickering stimulus) and a difference-of-Gaussian curve fit (black) for estimating the latency of the first peak. *B*: Power spectra of the example filter in A, based on the curve fit, for estimating the peak frequency. *C,D*: Population data of the peak latencies (C) and frequencies (D) across different conditions (light green, biphasic ON; dark green, monophasic ON; pink, biphasic OFF; violet, monophasic OFF). Here and thereafter, ***, $p < 0.001$; **, $p < 0.01$; *, $p < 0.05$; ns, non-significant (*t*-test). The filter types were identified by the quadrants of the PCA biplot (see Methods for details). *E-H*: Population data of the temporal filters across different conditions: from top to bottom, isoflurane anesthesia (E, $p < N = 213$), FMM anesthesia (F, $N = 69$), *ex vivo* (G, $N = 342$) and awake (H, $N = 71$). The four filter types are indicated on the right with corresponding colors.

Higher spiking activity in awake condition than *ex vivo*

How does a recording condition affect the firing properties of RGCs? The mean firing rate during the white-noise stimulus presentation was significantly higher in awake (35.0 ± 27.3 Hz; mean ± standard deviation) than in all the other recording conditions (isoflurane, 11.0 ± 10.2 Hz; FMM, 10.9 ± 10.7 Hz; *ex vivo*, 6.9 ± 6.6 Hz; all with $p < 0.001$, *t*-test in the logarithmic scale; Figure 6A). Importantly, this is not due to differences in the stimulus condition because the light intensity level was overall comparable between the recording setups (*in vivo*, ~16 $\mathrm{mW/m^2}$ on average at the eye; *ex vivo*, ~18 $\mathrm{mW/m^2}$ on the isolated retina; see Methods for details).

For a further analysis, we examined the static nonlinear gain function of the recorded cells (Eq. (7) in Methods). This gain function accounts for nonlinearity associated with spike generation, such as spike threshold and firing rate saturation, and is generally well explained by a sigmoid function (see Figure 6B for example). For quantification, we assessed the neutral firing rate of the cells where the input to the gain function is zero, i.e., the firing rate in the presence of “neutral” stimuli that are orthogonal to the cell’s STA. Consistent with the results

on the baseline firing rates measured by the sinusoidally flickering stimuli (Figure 3), the neutral firing rate was significantly higher in the awake condition (29.5 ± 25.4 Hz, mean ± standard deviation) than those under anesthesia (isoflurane, 7.6 ± 8.4 Hz, $p < 0.001$, *t*-test on a log scale; FMM, 7.5 ± 9.3 Hz, $p < 0.001$; Figure 6C). We also found that the neutral firing rates *ex vivo* (5.5 ± 7.1 Hz) were as low as those in the anesthetized conditions (isoflurane, $p = 0.02$; FMM, $p = 0.1$), and significantly lower than those in the awake condition ($p < 0.001$).

We further identified two distinct features in the gain function properties between *ex vivo* and *in vivo* responses. First, ON cell types generally had a higher gain than OFF cell types *ex vivo* (Figure 6F), whereas such cell-type specific differences were not observed *in vivo* (isoflurane, Figure 6D; FMM, Figure 6E; awake, Figure 6G). Second, the midpoint of the sigmoid fitted to *ex vivo* responses (1.6 ± 1.4, median ± interquartile range) was significantly higher than that for *in vivo* responses (isoflurane, 1.1 ± 0.9; FMM, 1.1 ± 0.8; awake, 0.9 ± 1.2; all with $p < 0.001$, Mann-Whitney *U*-test; Figure 6H). Taken together with the outcomes obtained with the sinusoidally flickering stimulus (Figure 3), this suggests that *in vivo* responses are more linearized to cover a larger dynamic range, especially in the awake condition due to high neutral responses (Figure 6G).

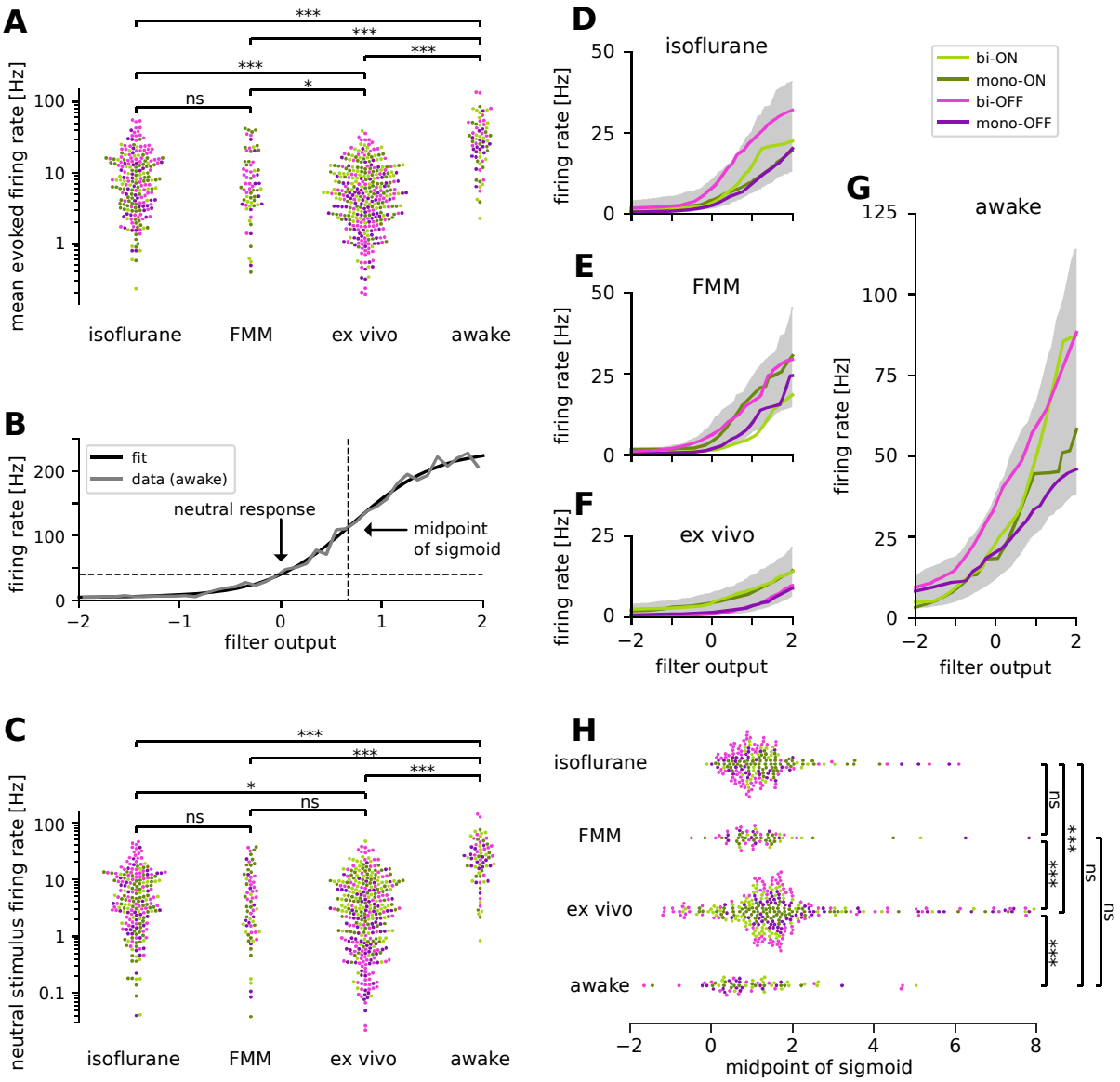

Figure 6: Retinal ganglion cells showed higher firing activity in awake condition than in anesthetized or *ex vivo* conditions. Cell types are color-coded as in Figure 5 (light green, biphasic ON; dark green, monophasic ON; pink, biphasic OFF; violet, monophasic OFF). *A*: Population data of the mean firing rates during the stimulus presentation period in four different recording conditions (isoflurane, FMM, *ex vivo*, and awake): ***, $p < 0.001$; **, $p < 0.01$; *, $p < 0.05$; ns, non-significant (*t*-test on the logarithm of firing rates). *B*: Static nonlinear gain function of a representative awake cell (the same one as in Figure 5A), estimated by the stimulus ensemble statistical techniques applied to the responses to a full-field randomly flickering stimulus (gray, Eq.(7) in Methods; black, sigmoid curve fit with the midpoint at 0.71). Note a high neutral stimulus response (40 Hz) defined as the firing rate at zero filter output (i.e., in the presence of stimuli orthogonal to the cell's STA). *C*: Population data of the neutral stimulus responses in each recording condition (in the same format as in A). *D-G*: Population data of the static nonlinear gain function (median for each cell type in corresponding colors; gray, interquartile range of all cells) across different conditions: isoflurane anesthesia (D, $N = 213$), FMM anesthesia (E, $N = 69$), *ex vivo* (F, $N = 342$), and awake condition (G, $N = 71$). *H*: Population data of the midpoint of the sigmoid nonlinearity in each recording condition: ***, p<0.001; Mann-Whitney *U*-test.

Discussion

Here we established optic tract recordings in head-fixed mice (Figure 1) and systematically analyzed the retinal output properties *in vivo* using a standardized set of visual stimuli for characterizing retinal functions (Baden et al., 2016; Jouty et al., 2018). We found that awake response properties were overall similar to those under isoflurane or FMM anesthesia (Figures 2-4) or *ex vivo* (Figures 5 and 6); however, we identified two distinct features in the awake condition: higher firing rates (Figures 3 and 6) and faster response dynamics (Figures 4 and 5). The change in the kinetics likely arose as a direct consequence of the high baseline activity in awake animals. When cells are on average more depolarized, it is faster to reach the spike threshold upon stimulation, hence leading to a shorter response latency (Zohar et al., 2011). High firing activity in awake animals has been widely observed in many brain areas across species (Greenberg et al., 2008; Sellers et al., 2015; Durand et al., 2016; Wright et al., 2017; De Franceschi and Solomon, 2018; Chen and Song, 2019). Therefore, the retinal response characteristics we observed *in vivo* could be a general feature of the brain in an awake state.

In awake animals, both the baseline and visually-evoked firing rates of RGCs were much higher—on average by ~20 Hz—than in those under anesthesia or in an isolated preparation (Figures 3 and 6). As a result, many awake ON cells showed OFF-suppressive responses, a new response type observed only in those cells with high baseline firing rates (~60 Hz). Here we classified these cells separately from the other ON cells in our clustering analysis (Figure 2); however, it is unlikely that they form a distinct “cell type” in the retina. Instead, these cells likely belong to a known cell type, and altered their response properties due to an increased baseline activity in the awake condition. Possible candidate cell types are: transient ON alpha cells (although they have a low baseline firing rate *ex vivo*; Krieger et al., 2017), ON contrast suppressive cells (although a sharp rebound response is missing in the calcium dynamics *ex vivo*; Baden et al., 2016), or suppressed-by-contrast cells (although their high baseline activity is suppressed by both ON and OFF stimuli; Mastronarde, 1985; Tien et

al., 2015; Jacoby and Schwartz, 2018). It is interesting to identify the exact cell type of these RGCs and further characterize their function *in vivo* in future studies.

What are the mechanisms underlying such differences between *in vivo* and *ex vivo* retinal responses? One possibility is the difference in the physiological states of the retina. Even if *ex vivo* recordings are made under a proper temperature using a perfusion medium specifically formulated to support isolated retinal tissues (Ames and Nesbett, 1981), there are certain unavoidable differences to the physiological condition *in vivo*. In particular, the retinal pigment epithelium, a key player for the visual cycle and spatial buffering of ions, is often removed in an isolated retinal preparation. A lack of retinal supply can then alter the physiological states of the retinal neurons, potentially leading to a change in their visual response properties.

Differences in the input stimulus properties, in contrast, cannot explain our results, even though retinal responses depend a lot on stimulus conditions. For example, the higher the light intensity level is, the higher the temporal frequency sensitivity becomes for *ex vivo* RGC responses (threshold at around 20-30 Hz; Wang et al., 2011) and so does the critical flicker-fusion frequency at the behavioral level (15-40 Hz; Umino et al., 2018; Nomura et al., 2019). Response latencies depend also on the spatial patterns of stimuli as well as their contrast (Bolz et al., 1982; Baccus and Meister, 2002; Sagdullaev and McCall, 2005; Pearson and Kerschensteiner, 2015; Tikidji-Hamburyan et al., 2015). Here we used full-field stimuli at slightly lower light intensity level for *in vivo* recordings than for *ex vivo* ones (see Methods for details). Therefore, higher baseline activity and faster dynamics observed in awake animals cannot be simply attributed to the difference in the stimulus conditions.

Finally, when comparing retinal responses across different studies, one cannot ignore a possible effect of sampling bias because visual response dynamics are cell-type specific (van Wyk et al., 2009; Krieger et al., 2017; Ravi et al., 2018; Tengölics et al., 2019). In an extreme case, delayed ON cells have the response latency slower than other RGC types by hundreds of milliseconds in an isolated mouse retina (Mani and Schwartz, 2017). Response

dynamics are also species-specific. For example, ON RGCs show higher baseline activity and faster responses than OFF cells in the macaque (Chichilnisky and Kalmar, 2002) and guinea pig (Zaghloul et al., 2003) retinas, whereas slower in the salamander retina (Gollisch and Meister, 2008), and such asymmetry between ON and OFF dynamics is pathway-specific in the rat retina (Ravi et al., 2018). Moreover, kinetics can vary even for the same cell type, depending on the retinal location (Warwick et al., 2018) or light-adaptation state (Chang and He, 2014; Tengölics et al., 2019). Sampling bias can then skew the results in many different ways. In this study, however, we recorded a wide variety of cell types (Figure 2), and no apparent difference was found in the STA distributions across different recording conditions (Figure 5). We thus expect that the effects of sampling bias should be minimal on the observed differences between *in vivo* and *ex vivo* retinal response characteristics.

Taken together, our findings indicate that clear differences exist in retinal physiology between *in vivo* and *ex vivo*. This highlights the importance of studying retinal function *in vivo*, especially in the awake condition.

Implications on retinal coding *in vivo*

The optic nerve fiber forms an information bottleneck in the early visual system. The human retina, for example, contains $\sim 10^8$ input neurons (photoreceptors) but only $\sim 10^6$ output neurons (RGCs) whose axons make up the optic nerve (Masland, 2012; Sanes and Masland, 2015). The retina is then expected to optimize the channel capacity by compressing the visual information as much as possible and conveying signals to the brain using as few spikes as possible (Attneave, 1954; Barlow and Rosenblith, 1961; Laughlin, 2001). Such an efficient coding hypothesis is well supported by both *ex vivo* experimental data and theoretical analyses. Under *ex vivo* conditions, RGCs are silent most of the time and fire spikes at high rates only when their selective stimulus features are presented (Gollisch and Meister, 2010; Baden et al., 2016; Jouty et al., 2018). This sparse RGC response, ensured by low spontaneous activity and strong nonlinearity (Pitkow and Meister, 2012), helps achieve high

efficiency and low redundancy in the visual representation of the retina (Doi et al., 2012). Furthermore, efficient coding principles can explain various physiological properties of the retina, such as separation of retinal outputs into multiple cell types (Gjorgjieva et al., 2019).

The retinal output characteristics we observed *in vivo*, however, provide a completely different view on the retinal code. First, unlike *ex vivo* conditions, RGCs in awake mice showed a high baseline activity with more linearized responses (Figures 3 and 6). Consequently, many awake ON cells primarily encoded light decrements by suppression from high baseline, rather than light increments by activation from low baseline. These cells convey the same information as conventional ON cells do—the more spikes, the higher light intensity—but using much more spikes. Thus, the amount of information transmitted per spike is much lower *in vivo* than *ex vivo*, violating the efficient coding principles. Second, we found less variability in the visual response dynamics across different RGC types *in vivo* (Figure 5E-H). This suggests that temporal coding framework based on spike timing patterns may not be readily applicable *in vivo*. Latency coding, for example, will not work well *in vivo* as it requires noticeable differences in the response latencies between two or more channels, such as ON and OFF pathways converging onto ON-OFF RGCs (Gollisch and Meister, 2008). Our results thus favor dense rate coding in the retina, rather than sparse temporal coding.

What are the advantages of such energy-inefficient retinal coding? As shown in our awake recordings, one can gain faster response kinetics (Figure 5) and wider bandwidths (Figure 6). In addition, redundancy in the dense code helps transmit signals accurately even with intrinsically noisy spike trains. These features are all highly beneficial from a behavioral viewpoint—e.g., to detect predators robustly and promptly—and thus worth achieving for survival at an expense of energy cost. Interestingly, dense coding can be a general feature of early sensory processing, as suggested by high baseline firing in vestibular and cochlear nuclei (Fuchs and Kimm, 1975; Rhode and Smith, 1986; Warchol and Dallos, 1990; Beraneck and Cullen, 2007), tonic activity in hair cells (Sachs and Abbas, 1974; Wu et al., 2016), and dark current in vertebrate photoreceptors (Hagins et al., 1970; Okawa et al., 2008). In fact, the

energy cost of dense retinal coding may not be so problematic with a relatively small number of neurons, as opposed to the total energy required for operating $\sim 10^9$ neurons in the cortex where sparse coding has certain advantages from the viewpoints of both energy efficiency and sensory processing (Olshausen and Field, 1996; Asari et al., 2006). Further characterizations of the retinal code *in vivo* will be needed to clarify what exactly the eye tells the brain.

Effects of anesthetics in early visual system

Anesthetics generally lower the excitability of nerve cells: e.g., isoflurane acts on the gamma-aminobutyric acid (GABA) type A receptors to silence the brain (Jenkins et al., 1999). It thus makes sense that the retinal outputs were reduced under anesthesia (Figures 3 and 6) and showed slower dynamics (Figures 4 and 5) than in awake animals. It is, however, difficult to generalize the effects of anesthesia because multiple mechanisms of action are involved, exerting complex effects on the sensory systems in anesthetic- and dose-dependent manners (Populin, 2005). For example, while visual cortical responses are reduced under anesthesia (Haider et al., 2013; Vaiceliunaite et al., 2013), auditory responses are enhanced (Raz et al., 2014; Sellers et al., 2015) and the response latency becomes shorter in the auditory pathway (Ter-Mikaelian et al., 2007).

Our results are nevertheless consistent with previous studies on the effects of anesthesia in the early visual system. Specifically, anesthesia reduces the overall activity of both SC and dLGN neurons, and leads to multiple changes in temporal processing of these two major retinorecipient areas, such as reduced sensitivity to high temporal frequencies and longer response latencies (Zhao et al., 2014; Durand et al., 2016; De Franceschi and Solomon, 2018). While different anesthetics were used in these studies (urethane as opposed to isoflurane and FMM), our consistent findings suggest that such changes in the response dynamics arise largely from the retina. In contrast, the effects of anesthesia on spatial response properties seem more complex. While spatial processing remains largely intact in

dLGN (Durand et al., 2016), lower contrast sensitivity and larger receptive field sizes were reported in SC under urethane anesthesia (De Franceschi and Solomon, 2018). Moreover, SC neurons show increased orientation selectivity under isoflurane anesthesia (Kasai and Isa, 2021). Here we also found a larger fraction of motion sensitive cells under both isoflurane and FMM anesthesia (Figure 2D-F). Due to confounding effects of eye movements in awake animals, however, we were not able to fully analyze spatial response properties of retinal outputs *in vivo*. It is a future challenge to develop algorithms to compensate for the eye motion at a spatial resolution well below the RGC receptive field size (as small as 3 degrees; Zhang et al., 2012) for fully characterizing spatiotemporal processing of the retina *in vivo*.

Materials and Methods

No statistical method was used to predetermine the sample size. The significance level was 0.05 (with Bonferroni correction where appropriate) in all analyses unless noted otherwise. All experiments were performed under the license 233/2017-PR from the Italian Ministry of Health. The data analyses were done in Python.

Animals

A total of 43 female C57BL/6J mice were used (chronic, 3; acute, 23; failures, 17, including 10 initial unsuccessful attempts to record from the optic chiasm) at around three months of age at the time of the surgery. Mice were kept on a 12-h light / 12-h dark cycle and given water and food *ad libitum*. After the chronic implantation of electrodes, the animals were kept single-housed.

Chronic recordings

For implanting electrodes, animals were anesthetized (induction, 4% isoflurane; maintenance, 1-2%) and placed inside a stereotaxic apparatus (Neurostar). Throughout the surgery, temperature was maintained at 37°C using a heating pad (Supertech Physiological), and eye ointment (VitA-POS) was used to prevent the eyes from drying. After positioning the mouse

head, the scalp skin was disinfected (Betadine) and removed with scissors. Soft tissue was removed from the skull surface with a round scalpel, and ethanol and acetone were applied to the skull for disinfection and removal of any residual compounds. The skull was glazed with a drop of cyanoacrylate adhesive (Loctite 401) to secure in place the surrounding skin, and then registered in the stereotaxic controller software (NeuroStar). A dental drill (WPI) was used to leave three marks on the skull to label the entry point for targeting the optic tract: [-1.34, +1.87, +4.74], [-1.70, +1.87, +4.74], and [-1.82, +2.35, +4.07] in [Anterior-Posterior, Medial-Lateral, Dorsal-Ventral] coordinates, respectively. A hole was drilled for a reference silver wire (A-M Systems) above the cerebellum, and the wire was inserted sideways to avoid excessive brain damage. After covering the hole and wire with Vaseline, the wire was attached to the skull with cyanoacrylate adhesive and dental cement (Paladur, PALA). Subsequently, a custom-designed titanium head-plate was attached to the skull with dental cement, followed by a craniotomy (diameter, 1-2 mm) and durotomy. A chronic silicone probe (Buzsaki32L, NeuroNexus) was then inserted with the stereotaxic controller (75 µm/min) first to a depth of 2 mm, retracted by 1 mm to release pressure created by the initial brain entry, and then to a depth of 4.5 mm from the skull surface. After reaching the desired depth, a microdrive (dDrive, NeuroNexus) was attached to the skull with dental cement, and the probe was removed from its mount and covered with a protective cap. The cables and connectors were cemented to the cap and covered with paraffin film (Bemis, Parafilm) to prevent the mouse from damaging the implant.

After the surgery, the animals were kept on a heating pad (Sera, Thermo comfort mat S) until they recovered from anesthesia. During the next four days, the mice received an anti-inflammatory/antibiotic cocktail (Rimadyl/Baytril; 0.5 mg/mL each, 0.01 mL/g). The antibiotic (Baytril) was given for an additional three days through drinking water (0.17 mg/mL).

After a recovery period of five days, the mice were placed on a custom-made rotary treadmill (diameter, 20 cm) with their head fixed for the recordings (at most two times a day, each for <2 hours). During the initial sessions, we moved the probe until visual responses

were observed (Figure 1A-D). The electrophysiology data were recorded at 30 kHz from each recording site (SmartBox, NeuroNexus) together with synchronization pulses from the visual stimulation device (see below). In total, we made 17 recording sessions from 3 out of 6 animals, where up to 10 cells were simultaneously recorded in each session (4.4 ± 2.4 cells/session, mean ± standard deviation).

After all the recording sessions, the electrode position was verified histologically (e.g., Figure 1E). The mice were anesthetized (2.5% Avertin, 16 µL/g, intraperitoneal injection) and perfused with paraformaldehyde (PFA; 4% in phosphate buffer solution). The animal's head with the electrode left in position was collected without the skull base, and stored in fixative solution (4% PFA) at 4°C for at least four days. This helped the brain tissue harden around the silicon probe, hence leaving a visible mark after removing the probe. Harvested brain tissue was then coronally sliced with a vibratome (Leica, VT1000S; thickness, 150 µm) and imaged under a bright-field microscope (Leica, LMD7000).

Acute recordings

Animals were anesthetized and placed inside a stereotaxic apparatus with a heating pad as described above. A contact lens (diameter, 3 mm; Ocuscience) was used for the target eye to prevent it from drying. The scalp was removed, registered in the stereotaxic controller, and the three entry points for targeting the optic tract were marked with the stereotaxic drill. A well was made with dental cement around the marks later to hold saline solution on top of the brain. After a craniotomy (diameter, 2 mm), an acute silicone probe (Buzsaki32L, Neuronexus) coated with a fluorescent dye (DiI stain, Invitrogen, D282) was slowly inserted into the brain (100 µm/min) with a micromanipulator (Sensapex, SMX) attached to the stereotaxic apparatus. While approaching the target depth, visual stimuli were presented (full-field contrast-inverting stimulus at 0.5 Hz; see below). The probe was moved until a maximum number of visually responsive cells were seen at once (up to 20 cells; 7.7 ± 5.3 cells/session, mean ± standard deviation; 52 sessions in total from 23 out of 27 animals).

Throughout the recordings, the mouse was kept under anesthesia with 1% isoflurane. The depth of anesthesia was monitored by the breathing rate (~1 breath/s). Alternatively, we used a cocktail of fentanyl, medetomidine and midazolam (FMM) during the recordings. In this case, once the electrode was in position, an FMM solution (fentanyl, 0.05 mg/kg; medetomidine, 0.5 mg/kg; midazolam, 5 mg/kg; in 0.9% NaCl saline) was intraperitoneally administered, and the isoflurane dose was progressively decreased to 0%. Buprenorphine (0.1 mg/kg) was injected 20 minutes after the termination of isoflurane, and the recording session was initiated 10 minutes after the buprenorphine injection. The depth of anesthesia was monitored through the heart rate (below around 300 beats per minute) and supplemental FMM anesthesia was provided when required. The electrophysiology data and the visual stimulation signals were recorded at 30 kHz/electrode (SmartBox, NeuroNexus).

At the end of the recording session, the electrode location was verified histologically. After retracting the silicone probe, the animal was perfused as described above. The brain tissue was harvested and post-fixed overnight in 4% PFA at 4°C. Coronal sections of the brain tissue (thickness, 150 µm) were then examined under a fluorescence microscope (Leica, LMD7000 with N2.1 filter cube) to visualize the trace left by the DiI stain on the probe.

Visual stimulation

Visual stimuli were presented by a custom gamma-corrected digital light processing (DLP) device (Texas Instruments, DLPDLCR3010EVM-LC) where the original green and red light-emitting diodes (LEDs) were replaced with ultra-violet (UV; 365 nm; LZ1-00UV00, LED Engine) and infrared (IR; 950 nm; SFH 4725S, Osram) LEDs, respectively. The UV and blue (465 nm) lights were projected onto a spherical screen (radius, 20 cm) with UV-reflective white paint (waterfowl store) placed ~20 cm to the contralateral side of an animal's eye from the implanted probe (Figure 1A), whereas the IR light was used as synchronization pulses, recorded via a photodiode with a custom transimpedance amplifier. The visual stimuli (1280-by-720 pixels; frame rate, 60 Hz) covered 73° in azimuth and 44° in altitude from the mouse

eye position (Figure 1B). The maximum light intensity at the eye position was 15.4 mW/m^2 and 15.9 mW/m^2 for the UV and blue LEDs, respectively, leading to mesopic to photopic conditions.

Using this DLP setup and QDSpy software (Franke et al., 2019), we presented the following set of visual stimuli: a randomly flickering full-field stimulus (5 min; 60 Hz), a moving grating stimulus (spatial frequencies of square waves, 3° or 20°; moving speed, 7.5°/s or 15°/s, in eight different directions), a full-field stimulus whose intensity followed a sinusoid (1.5 Hz) with a linearly increasing amplitude from 0% to 100% contrast over 10 s (10 trials; Figure 3), and a full-field sinusoidally flickering stimulus (maximum contrast) at different temporal frequencies (1.875, 3.75 and 7.5 Hz, each for 2 s; 15 Hz for 1 s; 10 trials; Figure 4). The last two full-field stimuli were preceded by a sequence of "OFF-ON-OFF" stimulation at maximum contrast (full-field contrast inversion; 2 s each) and interleaved by a 1-s-long gray screen across trials. These stimuli were equivalent to those used for differentiating ~30 RGC types *ex vivo* (Baden et al., 2016; Jouty et al., 2018).

Data analysis

Spike sorting was performed with SpykingCircus (Yger et al., 2018) for semi-automatic cluster detection and Phy (Rossant, 2020) for data curation. In total, we obtained 75 cells for chronic recordings, and 298 and 103 cells for acute recordings under isoflurane and FMM anesthesia, respectively. Not all cells responded to the entire stimulus set, but cells responding to any of the presented stimuli were included in the analysis. For *ex vivo* recordings, we reanalyzed the data sets in Vlasiuk and Asari (2021). Specifically, the *ex vivo* data sets included the activity of 696 cells recorded with a multi-electrode array (from 18 isolated mouse retinas) in response to a randomly flickering full-field visual stimulus projected from a gamma-corrected cathode-ray tube monitor (frame rate, 100 Hz) or a DLP device (60 Hz). The maximum light intensity on the isolated retinas was 36 mW/m^2 (Vlasiuk and Asari, 2021).

Response quality

We assessed the cell's response quality based on the trial-to-trial reliability of the response $r(t)$ during the "ON-OFF" period of the OFF-ON-OFF stimulus sequence (see Figure 2A for example). Specifically, the signal-to-noise ratio was calculated for each cell as follows:

$$\mathrm{SNR} = \frac{\mathrm{var}[\langle r(t) \rangle]_t}{\langle \mathrm{var}[r(t)]_t \rangle}, \quad (1)$$

where $\langle \cdot \rangle$ indicates the mean over trials, and $\mathrm{var}[\cdot]_t$ the variance over time t (bin size, $\Delta t = 16.6$ ms). We set a threshold at 0.15 to select reliably responsive cells for further analyses (Figure 2B).

Response polarity

To characterize the cell's preference to stimulus polarity, we defined an ON-OFF index using the responses to the full-field contrast inversion:

$$\text{ON-OFF index} = \frac{r_{\mathrm{ON}} - r_{\mathrm{OFF}}}{r_{\mathrm{ON}} + r_{\mathrm{OFF}}}, \quad (2)$$

where r_{ON} and r_{OFF} are the mean firing rate during the ON and the second OFF periods of the OFF-ON-OFF stimulus sequence, respectively. Positive and negative ON-OFF index values indicate stronger responses to ON and OFF stimuli, respectively (Figure 2C).

Motion sensitivity

Direction-selectivity (DS) and orientation-selectivity (OS) indices were calculated by projecting the responses to the moving grating stimuli onto a complex exponential:

$$\text{DS or OS index} = \left\| \frac{\sum_k e^{-i\alpha\omega_k} \cdot r_k}{\sum_k r_k} \right\|, \quad (3)$$

where ω_k and r_k are the angle of the k-th direction and the cell's corresponding responses, respectively; and $\alpha = 1$ and 2 for the DS and OS indices, respectively. Cells were considered motion-sensitive when at least one of these indices was higher than 0.15 and $p < 0.2$ calculated by bootstrap methods (1,000 repetitions; Figure 2D-F).

Temporal frequency sensitivity

Temporal frequency sensitivity was assessed by fitting an even power of sine function to the responses to the full-field sinusoidally flickering stimulus at different frequencies h (1.875, 3.75, 7.5, or 15 Hz; Figure 4):

$$s(t) = A \cdot \sin^q\left(\pi h t - \frac{\phi}{2}\right) + B, \tag{4}$$

where A and $B \geq 0$ are the response amplitude and baseline activity, respectively; and $q = 2n$ with $n \in \mathbb{N}^+$ is the exponent of the sine function. The phase $\phi \in [-\pi, \pi)$ indicates the relative position between the response peak and the sinusoidal stimulus patterns. For example, $\phi = -\pi/2$ and $\pi/2$ are obtained if the response reaches its peak when the stimulus is brightest and darkest, respectively.

The fit quality was then assessed by the explained variance:

$$R^2 = 1 - \frac{\mathrm{var}[\mathrm{Data} - \mathrm{Fit}]}{\mathrm{var}[\mathrm{Data}]}. \tag{5}$$

We set a threshold at 0.2 to select cells with a good fit hence responsive to the stimulus (Figure 4C), and compared the proportions of the responsive cells across different recording conditions (two-proportion z-test; Figure 4D).

Contrast sensitivity

We used a sigmoid-weighted sine-power function to characterize the responses to the flickering stimulus ($h = 1.5$ Hz) with increasing contrast (Figure 3):

$$S(t) = \frac{A}{1 + e^{-\lambda(t - t_0)}} \cdot \sin^q\left(\pi h t - \frac{\phi}{2}\right) + B, \tag{6}$$

where t_0 and $\lambda > 0$ are the midpoint and the steepness of the sigmoid, respectively; and the other free parameters are the same as $s(t)$ in Eq.(4). The fitted parameter values were then compared across different recording conditions (Mann-Whitney U-test for the baseline B, Figure 3D; Levene F-test for the amplitude A, Figure 3E; and t-test for the phase ϕ, Figure

677 3F). As a measure of contrast sensitivity, we used an estimated response magnitude at 10%
678 contrast from Eq.(6).

679 Temporal filters and static nonlinear gain functions

680 For systematically characterizing the response dynamics, we used stimulus ensemble
681 statistical techniques ("reverse correlation" methods; 500 ms window) to calculate the linear
682 filter (Figure 5) and static nonlinear gain function (Figure 6) of the recorded cells in response
683 to a randomly flickering visual stimulus (Meister et al., 1994; Chichilnisky, 2001). First, we
684 obtained the linear filter of each cell by calculating a spike-triggered average (STA) of the
685 stimulus with ± 1 being "white" and "black," respectively. As a quality measure, p-value was
686 computed for each time bin against a null hypothesis that the STA follows a normal distribution
687 with a mean of zero and a variance of $1/C$, where C is the total number of spikes. As a
688 measure of the cell's temporal frequency tuning, we then estimated the peak latency by fitting
689 a difference-of-Gaussian curve to the linear filter (e.g., Figure 5A); and the spectral peak
690 frequency by the Fourier analysis on the fitted curve (e.g., Figure 5B). The curve fitting quality
691 was assessed by the explained variance R^2 as in Eq. (5). We discarded the cells if $p > 10^{-18}$
692 for all time bins or $R^2 < 0.8$. We ran a t-test to compare the temporal frequency tuning
693 properties at the population level across recording conditions (Figure 5C,D) or across different
694 cell types in each recording condition (Figure 5E-H). Spatial response properties were not
695 examined in this study because complex nonlinear kinematics of eye movements in the awake
696 condition precluded the analysis at a high enough spatial resolution; and because it has been
697 shown that anesthesia has no effect on the spatial processing in dLGN, a direct downstream
698 of the retina (Durand et al., 2016).

699 Static nonlinear gain function $P(\mathrm{response}|\mathrm{stimulus})$ of each cell was computed by
700 taking the ratio between the distribution of spike-triggered stimulus ensembles
701 $N(\mathrm{stimulus}|\mathrm{response})$ projected onto the $L2$-normalized STA (bin size, 0.1) and that of the
702 entire stimulus ensembles $N(\mathrm{stimulus})$ (e.g., Figure 6B):

$$P(\text{response}|\text{stimulus}) = \frac{N(\text{stimulus}|\text{response})}{N(\text{stimulus})}/\Delta t\,. \quad (7)$$

A sigmoid function was fitted to $P(\text{response}|\text{stimulus})$ for smoothing. The neutral stimulus response was then defined as the vertical-intercept of the sigmoid function at the horizontal axis value of zero: i.e., the firing rate when the stimulus is orthogonal to the STA. We ran a t-test to compare the neutral stimulus responses and the average firing rates during the stimulus presentation at the population level across conditions (Figure 6A,C); and Mann-Whitney *U*-test to compare the midpoint of the sigmoid (Figure 6H).

Cell-type classification

In this study, we were not able to perform a morphological analysis of individual cells as we employed blind *in vivo* recording methods (Figure 1). We thus focused on the visual response properties for classifying cell-types in the following two ways.

First, we classified cells *in vivo* using the response quality, response polarity, and motion sensitivity (Figure 2). Specifically, we first divided the cells into two groups: reliably responsive ones with $\text{SNR} > 0.15$ (Eq. (2)) and the other low quality ones ("N/A" type; Figure 2B). We then set thresholds at ± 0.25 for the ON-OFF index (Eq. (3)) to identify ON, OFF, and ON/OFF types within the reliably responsive cells that increased firing in response to light increments, light decrements, and both, respectively (Figure 2C). For some cells where these measures were not available, we used the responses to the full-field sinusoidally flickering stimuli to calculate the response quality and polarity in a similar manner. Within the ON cells, we further identified an "OFF-suppressive" type if they had a significant negative amplitude in Eq. (6) with 95% confidence intervals in the parameter estimation. Independently, we also labeled cells as motion sensitive or not, based on the DS/OS indices as described above (Eq.(3); Figure 2D-F).

Second, because these measures are not available for the *ex vivo* data sets (Vlasiuk and Asari, 2021), we performed cell-type classification using the temporal filter properties to make a fair comparison between the *ex vivo* and *in vivo* data sets (Figures 5 and 6).

729 Specifically, we first ran a principal component analysis (PCA) on the temporal filters ($L2$-
730 normalized STA) obtained in each condition (Gollisch and Meister, 2008; Asari and Meister,
731 2014). The first two principal components (PC1, monophasic filter; and PC2, biphasic filter)
732 were largely sufficient to fit all the temporal filter dynamics, accounting for 78-86% of the total
733 variance in each condition. Each temporal filter is a point in the PCA biplot (i.e., the two-
734 dimensional space spanned by PC1 and PC2), and we grouped its shape into four subtypes
735 based on its position: monophasic OFF, biphasic OFF, monophasic ON, and biphasic ON from
736 the first to the fourth quadrants, respectively.

737 Acknowledgments

738 This work was supported by research grants from EMBL (H.A.). The EMBL Histology Facility
739 and the Advanced Light Microscopy Facility are acknowledged for support in sample
740 preparation and image acquisition for histological analyses, respectively. EMBL IT Support is
741 acknowledged for provision of computer and data storage servers. We thank Dmitry Molotkov
742 for his help in setting up the recording rig, and all the Asari lab members as well as Cornelius
743 Gross and Santiago Rompani for many useful discussions.

744 References

745 Ames, A., Nesbett, F. B. (1981). In Vitro Retina as an Experimental Model of the Central
746 Nervous System. J Neurochem, 37(4), 867-877.

747 Asari, H., Meister, M. (2014). The projective field of retinal bipolar cells and its modulation
748 by visual context. Neuron, 81(3), 641-652.

749 Asari, H., Pearlmutter, B. A., Zador, A. M. (2006). Sparse representations for the cocktail
750 party problem. J Neurosci, 26(28), 7477-7490.

751 Atick, J. J., Redlich, A. N. (1990). Towards a Theory of Early Visual Processing. Neural
752 Comput, 2(3), 308-320.

753 Attneave, F. (1954). Some informational aspects of visual perception. Psychol Rev, 61(3),
754 183-193.

755 Baccus, S. A., Meister, M. (2002). Fast and slow contrast adaptation in retinal circuitry.
756 Neuron, 36(5), 909-919.

757 Baden, T., Berens, P., Franke, K., Rosón, M. R., Bethge, M., Euler, T. (2016). The
758 functional diversity of retinal ganglion cells in the mouse. Nature, 529(7586), 345-350.

759 Barlow, H. B., Hill, R. M., Levick, W. R. (1964). Retinal ganglion cells responding
760 selectively to direction and speed of image motion in the rabbit. J Physiol, 173(3), 377-407.

761 Barlow, H. B., Rosenblith, W. A. (1961). Possible principles underlying the transformations
762 of sensory messages. In Sensory Communication (pp. 217-234). MIT Press.

763 Beraneck, M., and Cullen, K. E. (2007). Activity of vestibular nuclei neurons during
764 vestibular and optokinetic stimulation in the alert mouse. J Neurophysiol, 98(3), 1549-1565.

765 Bishop, P. O., Burke, W., Davis, R. (1962). The interpretation of the extracellular response
766 of single lateral geniculate cells. J Physiol (Lond), 162, 451-472.

767 Bolz, J., Rosner, G., Wässle, H. (1982). Response latency of brisk-sustained (X) and brisk-
768 transient (Y) cells in the cat retina. J Physiol, 328, 171-190.

769 Chang, L., He, S. (2014). Light adaptation increases response latency of alpha ganglion
770 cells via a threshold-like nonlinearity. Neuroscience, 256, 101-116.

771 Chen, C., Song, S. (2019). Differential cell-type dependent brain state modulations of
772 sensory representations in the non-lemniscal mouse inferior colliculus. Commun Biol, 2,
773 356.

774 Chichilnisky, E. J. (2001). A simple white noise analysis of neuronal light responses.
775 Network, 12(2), 199-213.

776 Chichilnisky, E. J., Kalmar, R. S. (2002). Functional asymmetries in ON and OFF ganglion
777 cells of primate retina. J Neurosci, 22(7), 2737-2747.

778 De Franceschi, G., Solomon, S. G. (2018). Visual response properties of neurons in the
779 superficial layers of the superior colliculus of awake mouse. J Physiol, 596(24), 6307-6332.

780 Doi, E., Gauthier, J. L., Field, G. D., Shlens, J., Sher, A., Greschner, M., Machado, T. A.,
781 Jepson, L. H., Mathieson, K., Gunning, D. E., Litke, A. M., Paninski, L., Chichilnisky, E. J.,
782 Simoncelli, E. P. (2012). Efficient Coding of Spatial Information in the Primate Retina. J
783 Neurosci, 32(46), 16256-16264.

784 Dombeck, D. A., Khabbaz, A. N., Collman, F., Adelman, T. L., Tank, D. W. (2007). Imaging
785 large-scale neural activity with cellular resolution in awake, mobile mice. Neuron, 56(1),
786 43-57.

787 Durand, S., Iyer, R., Mizuseki, K., de Vries, S., Mihalas, S., Reid, R. C. (2016). A
788 Comparison of Visual Response Properties in the Lateral Geniculate Nucleus and Primary
789 Visual Cortex of Awake and Anesthetized Mice. J Neurosci, 36(48), 12133-12156.

790 Enroth-Cugell, C., Robson, J. G. (1966). The contrast sensitivity of retinal ganglion cells
791 of the cat. J Physiol, 187, 517-552.

792 Esposti, F., Johnston, J., Rosa, J. M., Leung, K.-M., Lagnado, L. (2013). Olfactory
793 Stimulation Selectively Modulates the OFF Pathway in the Retina of Zebrafish. Neuron,
794 79(1), 97-110.

795 Franke, K., Chagas, A. M., Zhao, Z., Zimmermann, M. J., Bartel, P., Qiu, Y., Szatko, K. P.,
796 Baden, T., Euler, T. (2019). An arbitrary-spectrum spatial visual stimulator for vision
797 research. Elife, 8, e48779.

798 Fuchs, A. F., Kimm, J. (1975). Unit activity in vestibular nucleus of the alert monkey during
799 horizontal angular acceleration and eye movement. J Neurophysiol, 38(5), 1140-1161.

800 Geng, Y., Dubra, A., Yin, L., Merigan, W. H., Sharma, R., Libby, R. T., Williams, D. R.
801 (2012). Adaptive optics retinal imaging in the living mouse eye. Biomed Opt Express, 3(4),
802 715-734.

803 Gjorgjieva, J., Meister, M., Sompolinsky, H. (2019). Functional diversity among sensory
804 neurons from efficient coding principles. PLoS Comput Biol, 15(11), e1007476.

805 Gollisch, T., Meister, M. (2008). Rapid neural coding in the retina with relative spike
806 latencies. Science, 319(5866), 1108-1111.

807 Gollisch, T., Meister, M. (2010). Eye Smarter than Scientists Believed: Neural
808 Computations in Circuits of the Retina. Neuron, 65, 150-164.

809 Greenberg, D. S., Houweling, A. R., Kerr, J. N. D. (2008). Population imaging of ongoing
810 neuronal activity in the visual cortex of awake rats. Nat Neurosci, 11(7), 749-751.

811 Hagins, W. A., Penn, R. D., Yoshikami, S. (1970). Dark Current and Photocurrent in Retinal
812 Rods. Biophys J, 10(5), 380-412.

813 Haider, B., Häusser, M., Carandini, M. (2013). Inhibition dominates sensory responses in
814 the awake cortex. Nature, 493(7430), 97-100.

815 Hartline, H. K. (1938). The response of single optic nerve fibers of the vertebrate eye to
816 illumination of the retina. Am J Physiol, 121, 400–415.

817 Hong, G., Fu, T.-M., Qiao, M., Viveros, R. D., Yang, X., Zhou, T., Lee, J. M., Park, H.-G.,
818 Sanes, J. R. (2018). A method for single-neuron chronic recording from the retina in awake
819 mice. Science, 360(6396), 1447-1451.

820 Jacoby, J., Schwartz, G. W. (2018). Typology and Circuitry of Suppressed-by-Contrast
821 Retinal Ganglion Cells. Front Cell Neurosci, 12, 269.

822 Jenkins, A., Franks, N. P., Lieb, W. R. (1999). Effects of temperature and volatile
823 anesthetics on GABA(A) receptors. Anesthesiology, 90(2), 484-491.

824 Jouty, J., Hilgen, G., Sernagor, E., Hennig, M. H. (2018). Non-parametric Physiological
825 Classification of Retinal Ganglion Cells in the Mouse Retina. Front Cell Neurosci, 12, 481.

826 Jun, J. J., Steinmetz, N. A., Siegle, J. H., Denman, D. J., Bauza, M., Barbarits, B., Lee, A.
827 K., Anastassiou, C. A., Andrei, A., Aydın, Ç., Barbic, M., Blanche, T. J., Bonin, V., Couto,
828 J., Dutta, B., Gratiy, S. L., Gutnisky, D. A., Häusser, M., Karsh, B., … Harris, T. D. (2017).
829 Fully Integrated Silicon Probes for High-Density Recording of Neural Activity. Nature,
830 551(7679), 232-236.

831 Kaplan, E., Shapley, R. (1984). The origin of the S (slow) potential in the mammalian lateral
832 geniculate nucleus. Exp Brain Res, 55(1), 111-116.

833 Kasai, M., Isa, T. (2021). Effects of light isoflurane anesthesia on organization of direction
834 and orientation selectivity in the superficial layer of the mouse superior colliculus. J
835 Neurosci, JN-RM-1196-21. DOI: 10.1523/JNEUROSCI.1196-21.2021

836 Kretschmer, F., Tariq, M., Chatila, W., Wu, B., Badea, T. C. (2017). Comparison of
837 optomotor and optokinetic reflexes in mice. J Neurophysiol, 118(1), 300-316.

838 Krieger, B., Qiao, M., Rousso, D. L., Sanes, J. R., Meister, M. (2017). Four alpha ganglion
839 cell types in mouse retina: Function, structure, and molecular signatures. PLoS One, 12(7),
840 e0180091.

841 Kuffler, S. W. (1953). Discharge patterns and functional organization of mammalian retina.
842 J Neurophysiol, 16(1), 37-68.

843 Laughlin, S. B. (2001). Energy as a constraint on the coding and processing of sensory
844 information. Curr Opin Neurobiol, 11(4), 475-480.

845 Lee, S.-H., Dan, Y. (2012). Neuromodulation of brain states. Neuron, 76(1), 209-222.

846 Lettvin, J. Y., Maturana, H. R., McCulloch, W. S., Pitts, W. H. (1959). What the frog's eye
847 tells the frog's brain. Proc Inst Radio Engr, 47, 1940-1951.

Li, J. Y., Schmidt, T. M. (2018). Divergent projection patterns of M1 ipRGC subtypes. J Comp Neurol, 526(13), 2010-2018.

Liang, L., Fratzl, A., Goldey, G., Ramesh, R. N., Sugden, A. U., Morgan, J. L., Chen, C., Andermann, M. L. (2018). A Fine-Scale Functional Logic to Convergence from Retina to Thalamus. Cell, 173(6), 1343-1355.e24.

Liang, L., Fratzl, A., Reggiani, J. D. S., Mansour, O. E., Chen, C., Andermann, M. L. (2020). Retinal Inputs to the Thalamus Are Selectively Gated by Arousal. Curr Biol, 30(20), 3923-3934.e9.

Mani, A., Schwartz, G. W. (2017). Circuit Mechanisms of a Retinal Ganglion Cell with Stimulus-Dependent Response Latency and Activation Beyond Its Dendrites. Curr Biol, 27(4), 471-482.

Masland, R. H. (2012). The Neuronal Organization of the Retina. Neuron, 76, 266-280.

Mastronarde, D. N. (1983). Correlated firing of cat retinal ganglion cells. I. Spontaneously active inputs to X- and Y-cells. J Neurophysiol, 49(2), 303-324.

Mastronarde, D. N. (1985). Two types of cat retinal ganglion cells that are suppressed by contrast. Vision Res, 25(9), 1195-1196.

Meister, M., Pine, J., Baylor, D. A. (1994). Multi-neuronal signals from the retina: acquisition and analysis. J Neurosci Methods, 51(1), 95-106.

Niell, C. M., Stryker, M. P. (2010). Modulation of visual responses by behavioral state in mouse visual cortex. Neuron, 65(4), 472-479.

Nomura, Y., Ikuta, S., Yokota, S., Mita, J., Oikawa, M., Matsushima, H., Amano, A., Shimonomura, K., Seya, Y., Koike, C. (2019). Evaluation of critical flicker-fusion frequency measurement methods using a touchscreen-based visual temporal discrimination task in the behaving mouse. Neurosci Res, 148, 28-33.

Okawa, H., Sampath, A. P., Laughlin, S. B., Fain, G. L. (2008). ATP Consumption by Mammalian Rod Photoreceptors in Darkness and in Light. Curr Biol, 18(24), 1917-1921.

Olshausen, B. A., Field, D. J. (1996). Emergence of simple-cell receptive field properties by learning a sparse code for natural images. Nature, 381(6538), 607-609.

Pearson, J. T., Kerschensteiner, D. (2015). Ambient illumination switches contrast preference of specific retinal processing streams. J Neurophysiol, 114(1), 540-550.

Pitkow, X., Meister, M. (2012). Decorrelation and efficient coding by retinal ganglion cells. Nat Neurosci, 15(4), 628-635.

Populin, L. C. (2005). Anesthetics Change the Excitation/Inhibition Balance That Governs Sensory Processing in the Cat Superior Colliculus. J Neurosci, 25(25), 5903-5914.

Ravi, S., Ahn, D., Greschner, M., Chichilnisky, E. J., Field, G. D. (2018). Pathway-Specific Asymmetries between ON and OFF Visual Signals. J Neurosci, 38(45), 9728-9740.

Raz, A., Grady, S. M., Krause, B. M., Uhlrich, D. J., Manning, K. A., Banks, M. I. (2014). Preferential effect of isoflurane on top-down vs. bottom-up pathways in sensory cortex. Front Syst Neurosci, 8, 191.

Repérant, J., Ward, R., Miceli, D., Rio, J. P., Médina, M., Kenigfest, N. B., Vesselkin, N. P. (2006). The centrifugal visual system of vertebrates: a comparative analysis of its functional anatomical organization. Brain Res Rev, 52(1), 1-57.

Rhode, W. S., and Smith, P. H. (1986). Encoding timing and intensity in the ventral cochlear nucleus of the cat. J Neurophysiol, 56(2), 261-286.

Rossant, C. (2020). Phy: interactive visualization and manual spike sorting of large-scale ephys data. GitHub. https://github.com/cortex-lab/phy

Sachs, M. B., Abbas, P. J. (1974). Rate versus level functions for auditory-nerve fibers in cats: tone-burst stimuli. J Acoust Soc Am, 56(6), 1835-1847.

Sagdullaev, B. T., McCall, M. A. (2005). Stimulus size and intensity alter fundamental receptive-field properties of mouse retinal ganglion cells in vivo. Vis Neurosci, 22(5), 649-659.

Sanes, J. R., Masland, R. H. (2015). The types of retinal ganglion cells: current status and implications for neuronal classification. Annu Rev Neurosci, 38, 221-246.

Schröder, S., Steinmetz, N. A., Krumin, M., Pachitariu, M., Rizzi, M., Lagnado, L., Harris, K. D., Carandini, M. (2020). Arousal Modulates Retinal Output. Neuron, 107(3), 487-495.

Sellers, K. K., Bennett, D. V., Hutt, A., Williams, J. H., Fröhlich, F. (2015). Awake vs. anesthetized: layer-specific sensory processing in visual cortex and functional connectivity between cortical areas. J Neurophysiol, 113(10), 3798-3815.

Shekhar, K., Lapan, S. W., Whitney, I. E., Tran, N. M., Macosko, E. Z., Kowalczyk, M., Adiconis, X., Levin, J. Z., Nemesh, J., Goldman, M., McCarroll, S. A., Cepko, C. L., Regev, A., Sanes, J. R. (2016). Comprehensive Classification of Retinal Bipolar Neurons by Single-Cell Transcriptomics. Cell, 166(5), 1308-1323.e30.

Sibille, J., Gehr, C., Benichov, J. I., Balasubramanian, H., Teh, K. L., Lupashina, T., Vallentin, D., Kremkow, J. (2021). Strong and specific connections between retinal axon mosaics and midbrain neurons revealed by large scale paired recordings. bioRxiv. 10.1101/2021.09.09.459396

Strauss, O. (2005). The retinal pigment epithelium in visual function. Physiol Rev, 85(3), 845-881.

Tabata, H., Shimizu, N., Wada, Y., Miura, K., Kawano, K. (2010). Initiation of the optokinetic response (OKR) in mice. J Vis, 10(1), 1-17.

Tengölics, Á. J., Szarka, G., Ganczer, A., Szabó-Meleg, E., Nyitrai, M., Kovács-Öller, T., Völgyi, B. (2019). Response Latency Tuning by Retinal Circuits Modulates Signal Efficiency. Sci Rep, 9(1), 15110.

Ter-Mikaelian, M., Sanes, D. H., Semple, M. N. (2007). Transformation of temporal properties between auditory midbrain and cortex in the awake Mongolian gerbil. J Neurosci, 27(23), 6091-6102.

Tien, N.-W., Pearson, J. T., Heller, C. R., Demas, J., Daniel, K. (2015). Genetically Identified Suppressed-by-Contrast Retinal Ganglion Cells Reliably Signal Self-Generated Visual Stimuli. J Neurosci, 35(30), 10815-10820.

Tikidji-Hamburyan, A., Reinhard, K., Seitter, H., Hovhannisyan, A., Procyk, C. A., Allen, A. E., Schenk, M., Lucas, R. J., Münch, T. A. (2015). Retinal output changes qualitatively with every change in ambient illuminance. Nat Neurosci, 18(1), 66-74.

Umino, Y., Pasquale, R., Solessio, E. (2018). Visual Temporal Contrast Sensitivity in the Behaving Mouse Shares Fundamental Properties with Human Psychophysics. eNeuro, 5(4), ENEURO.0181-18.2018.

Vaiceliunaite, A., Erisken, S., Franzen, F., Katzner, S., Busse, L. (2013). Spatial integration in mouse primary visual cortex. J Neurophysiol, 110(4), 964-972.

van Wyk, M., Wässle, H., Taylor, W. R. (2009). Receptive field properties of ON- and OFF-ganglion cells in the mouse retina. Vis Neurosci, 26(3), 297-308.

Vidal-Sanz, M., Galindo-Romero, C., Valiente-Soriano, F. J., Nadal-Nicolás, F. M., Ortin-Martinez, A., Rovere, G., Salinas-Navarro, M., Lucas-Ruiz, F., Sanchez-Migallon, M. C., Sobrado-Calvo, P., Aviles-Trigueros, M., Villegas-Pérez, M. P., Agudo-Barriuso, M. (2017). Shared and Differential Retinal Responses against Optic Nerve Injury and Ocular Hypertension. Front Neurosci, 11, 235.

Vlasiuk, A., Asari, H. (2021). Feedback from retinal ganglion cells to the inner retina. PLoS One, 16(7), e0254611.

Wang, Y. V., Weick, M., Demb, J. B. (2011). Spectral and temporal sensitivity of cone-mediated responses in mouse retinal ganglion cells. J Neurosci, 31(21), 7670-7681.

946 Warchol, M. E., Dallos, P. (1990). Neural coding in the chick cochlear nucleus. J Comp
947 Physiol A, 166(5), 721-734.

948 Warwick, R. A., Kaushansky, N., Sarid, N., Golan, A., Rivlin-Etzion, M. (2018).
949 Inhomogeneous Encoding of the Visual Field in the Mouse Retina. Curr Biol, 28(5), 655-
950 665.e3.

951 Weyand, T. G. (2007). Retinogeniculate transmission in wakefulness. J Neurophysiol,
952 98(2), 769-785.

953 Wright, P. W., Brier, L. M., Bauer, A. Q., Baxter, G. A., Kraft, A. W., Reisman, M. D., Bice,
954 A. R., Snyder, A. Z., Lee, J.-M., Culver, J. P. (2017). Functional connectivity structure of
955 cortical calcium dynamics in anesthetized and awake mice. PLoS One, 12(10), e0185759.

956 Wu, J. S., Young, E. D., Glowatzki, E. (2016). Maturation of Spontaneous Firing Properties
957 after Hearing Onset in Rat Auditory Nerve Fibers: Spontaneous Rates, Refractoriness,
958 and Interfiber Correlations. J Neurosci, 36(41), 10584-10597.

959 Yan, W., Laboulaye, M. A., Tran, N. M., Whitney, I. E., Benhar, I., Sanes, J. R. (2020).
960 Mouse Retinal Cell Atlas: Molecular Identification of over Sixty Amacrine Cell Types. J
961 Neurosci, 40(27), 5177-5195.

962 Yger, P., Spampinato, G. L., Esposito, E., Lefebvre, B., Deny, S., Gardella, C., Stimberg,
963 M., Jetter, F., Zeck, G., Picaud, S., Duebel, J., Marre, O. (2018). A spike sorting toolbox
964 for up to thousands of electrodes validated with ground truth recordings in vitro and in vivo.
965 Elife, 7, e34518.

966 Yin, L., Geng, Y., Osakada, F., Sharma, R., Cetin, A. H., Callaway, E. M., Williams, D. R.,
967 Merigan, W. H. (2013). Imaging light responses of retinal ganglion cells in the living mouse
968 eye. J Neurophysiol, 109(9), 2415-2421.

969 Yin, L., Masella, B., Dalkara, D., Zhang, J., Flannery, J. G., Schaffer, D. V., Williams, D.
970 R., Merigan, W. H. (2014). Imaging light responses of foveal ganglion cells in the living
971 macaque eye. J Neurosci, 34(19), 6596-6605.

972 Zaghloul, K. A., Boahen, K., Demb, J. B. (2003). Different circuits for ON and OFF retinal
973 ganglion cells cause different contrast sensitivities. J Neurosci, 23(7), 2645-2654.

974 Zhang, Y., Kim, I.-J., Sanes, J. R., Meister, M. (2012). The most numerous ganglion cell
975 type of the mouse retina is a selective feature detector. Proc Natl Acad Sci U S A, 109(36),
976 E2391-E2398.

977 Zhao, X., Liu, M., Cang, J. (2014). Visual cortex modulates the magnitude but not the
978 selectivity of looming-evoked responses in the superior colliculus of awake mice. Neuron,
979 84(1), 202-213.

980 Zohar, O., Shackleton, T. M., Nelken, I., Palmer, A. R., Shamir, M. (2011). First spike
981 latency code for interaural phase difference discrimination in the guinea pig inferior
982 colliculus. J Neurosci, 31(25), 9192-9204.